applied sciences

MDPI

Article

A Photon Blockade in a Coupled Cavity System Mediated by an Atom

Ming-Cui Li [1] and Ai-Xi Chen [2,*]

[1] College of Information School, East China Jiaotong University, Nanchang 330013, China; cacaony@163.com
[2] School of Science, Zhejiang Sci-Tech University, Hangzhou 310018, China
* Correspondence: aixichen@zstu.edu.cn

Received: 15 January 2019; Accepted: 4 March 2019; Published: 8 March 2019

check for updates

Abstract: We investigate theoretically the photon statistics in a coupled cavity system mediated by a two-level atom. The system consists of a linear cavity weakly driven by a continuous laser, and a nonlinear cavity containing an atom inside. We find that there exists a photon blockade in the linear cavity for both parameter regimes where the coupling strength between the atom and the nonlinear cavity is greater (or less) than the dissipation rate of the linear cavity. We also extend our model by pumping the two cavities simultaneously and find that the conventional photon blockade is apparent in the linear cavity, whereas the unconventional photon blockade appears in the nonlinear cavity. These results show that our work has potential applications for a single photon source in a weakly nonlinear system.

Keywords: photon blockade; cavity; quantum coherent

1. Introduction

Single photon source and single photon detectors have great potential applications in precision measurement instruments, quantum information computing, and quantum communications [1,2]. For instances, in quantum information science, single photons can be promising quantum bits on which information can be encoded using interferometers or polarization, and can be used in quantum key distribution and other applications. In other domains, single photon detectors are used in a wide range of applications, such as bioluminescence detection, Deoxyribonucleic acid (DNA) sequencing, and picosecond imaging circuit analysis. Single photon emitters deliver photons one at a time, which is also called photon antibunching phenomenon [3]. This single photon is quantized by its energy $\hbar\nu_k$, where $\hbar$ is Planck's constant, and ν_k is the frequency of the kth mode in the quantized electromagnetic field. A single photon source can be generated by different mechanisms. Clauser [4] first generated single photons in 1974 based on a cascade transition of calcium atoms. Diedrich and Walther investigated the antibunching and sub-Poissonian properties of the resonance fluorescence of a single atomic ion stored in a radio-frequency trap [5]. Nano-objects in condensed matter are also possible sources of single photons [6], such as semiconductor nanocrystals [7], color centers in diamonds [8], and quantum dots [9–11].

In cavity quantum electrodynamics (QED), a photon blockade is typically achieved by the coupling of nonlinear freedoms that give rise to the anharmonicity of the Jaynes–Cummings ladder of the system eigenstates. A conventional photon blockade is the result of the strong nonlinearity of the system, which requires the single-photon nonlinearity to be at least larger than the mode linewidth κ [12–15]. A photon blockade created in weakly nonlinear systems, which are far more natural in many areas of photonics and are more feasible to integration and scalability, is referred to as an unconventional photon blockade (UPB) [16–18]. The underlying mechanism for the UPB is the destructive quantum interference between different excitation pathways, which usually requires that the system involves several degrees of freedom to establish multi-transition paths. The UPB was first put forward by Liew and Savona [16] in a pair of coupled quantum modes. The UPB has been, since then, studied in various cavity systems, such as two coupled Kerr nonlinear cavity structures with one laser-driven [19], one linear cavity coupled to a Kerr nonlinear cavity with one driving laser [20], two nonlinear cavities with two driving laser [21], two coupled Kerr cavities in a semiconductor [22] and in all-silicon [23], two overlapped cavities corresponding to low frequency and high frequency modes [24], and one cavity coupled to a quantum dot with two driving laser [25].

We know that physical mechanisms of conventional and unconventional photon blockades are different. For conventional photon blockades, the system needs to have a strong nonlinarity effect, whereas UPBs need a weak nonlinearity effect. For obtaining the unconventional photon blockade, we introduce a two-level atom system in Cavity B. We use a pump laser to couple the cavity field, and the interaction between the cavity and the atom can then be effectively manipulated, which provide a method for realization of the unconventional photon blockade. In this paper, we go back to the basic Jaynes–Cummings model and study the conventional and unconventional photon blockade effect in a linear cavity coupled to a nonlinear cavity. The nonlinearity of the second cavity is mediated by a two-level atom. An atom itself is a potential emitter of light, and the cavity can enhance the spontaneous emission rate and the photon production rate. The second cavity provides different transition paths for the photons in the first cavity. We find that there are conventional and unconventional photon blockade effects when the first cavity, the second cavity, and the atom are resonant with the driving laser. So far, the coexistence of two different photon blockades has not been reported. Laser manipulation and atomic coupling are relatively mature technologies, so our scheme is feasible in experiment. A photon blockade is an effective method for realization of a single photon source, which plays an important role in quantum communication and quantum information processing.

The rest of this paper is organized as follows. In Section 2, we introduce the model, the photon transition paths, and the ladder of the dressed states. In Section 3, we demonstrate the conventional and unconventional single photon blockade by numerically solving the master equation and calculating the equal-time second correlation function. In Section 4, we study the optimal parameters for equal-time second correlation function using the non-Hermitian effective Hamiltonian method. In Section 5, we provide some extension discussions of our proposal by adding a simultaneous pump laser to the nonlinear cavity. Conclusions are given in Section 6.

2. Model

As shown in Figure 1, we consider a coupled cavity system that consists of two cascaded cavities. The first cavity (Cavity A) is driven by a classical light field with frequency ω_L and amplitude ε. The Hamiltonian of Cavity A with the driven leaser is given by

$$H_A = \hbar\omega_a a^\dagger a + \hbar\varepsilon(a^\dagger e^{-i\omega_L t} + a e^{i\omega_L t}) \tag{1}$$

where a is the annihilation operator of Cavity A whose resonant frequency is ω_a, and $a^\dagger$ is the creation operator. We apply the rotating wave approximation. The Hamiltonian of the second cavity (Cavity B) reads as

$$H_B = \hbar\omega_b b^\dagger b + \hbar\omega_1 \sigma^\dagger \sigma + \hbar g(\sigma^\dagger b + \sigma b^\dagger) \tag{2}$$

Here, b and $b^\dagger$ are the annihilation operator and creation operator of the mode in Cavity B, whose resonant frequency is ω_b. The lowering (up) operator of the two-level atom in Cavity B is denoted by σ ($\sigma^\dagger$), and the transition frequency of the atom is ω_1. g describes the coupling strength between the atom and Cavity B. These two cavities are coupled through photon hopping interactions with strength of J.

In a rotating frame with respect to $H_0 = \hbar\omega_L a^\dagger a + \hbar\omega_L b^\dagger b + \hbar\omega_L \sigma^\dagger\sigma$, the Hamiltonian of the whole system is given by ($\hbar = 1$):

$$H = \Delta_a a^\dagger a + \Delta_b b^\dagger b + \Delta_1 \sigma^\dagger \sigma + g(\sigma^\dagger b + \sigma b^\dagger) + J(a^\dagger b + a b^\dagger) + \varepsilon(a^\dagger + a). \tag{3}$$

Δ_a, Δ_b and Δ_1 are, respectively, the frequency detuning of Cavity A, Cavity B, and the atom with respect to the driving field.

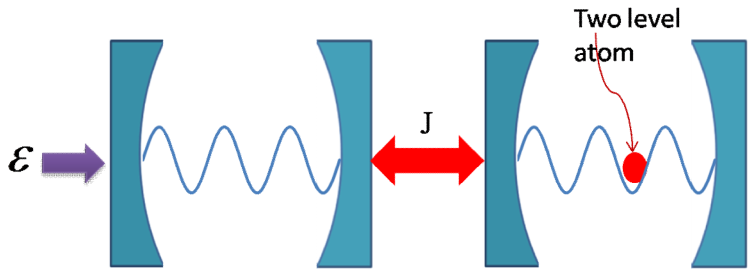

Figure 1. Schematic of the studied system. The system consists of two cavities, which are coupled to each other through a photon-hopping interaction. The first cavity is a linear cavity driven by a continuous laser. The second cavity is nonlinear with a two-level atom.

In the weak-driving regime, where the driving amplitude ε is far less than the dissipation rate of Cavity A, we consider the total excitation number $N \leq 2$ in our system. Then the bare states of the system are $|0,0,g\rangle$, $|0,0,e\rangle$, $|0,1,g\rangle$, $|1,0,g\rangle$, $|0,1,e\rangle$, $|1,0,e\rangle$, $|1,1,g\rangle$, $|0,2,g\rangle$, and $|2,0,g\rangle$, with the first number denoting the photon number in Cavity A, the second number denoting the photon number in Cavity B, and the third part denoting the status of the atom in Cavity B. For simplification, we denote these nine bare states by $|0\rangle$, $|1\rangle$, $\cdots$, $|8\rangle$, respectively. The Hamiltonian in Equation (3) without the driving field can be expressed in the following matrix:

$$\begin{bmatrix} 0 & 0 & 0 & 0 & 0 & 0 & 0 & 0 & 0 \\ 0 & \Delta_1 & g & 0 & 0 & 0 & 0 & 0 & 0 \\ 0 & g & \Delta_b & J & 0 & 0 & 0 & 0 & 0 \\ 0 & 0 & J & \Delta_a & 0 & 0 & 0 & 0 & 0 \\ 0 & 0 & 0 & 0 & \Delta_b + \Delta_1 & J & 0 & g & 0 \\ 0 & 0 & 0 & 0 & J & \Delta_a + \Delta_1 & g & 0 & 0 \\ 0 & 0 & 0 & 0 & 0 & g & \Delta_a + \Delta_b & J & J \\ 0 & 0 & 0 & 0 & g & 0 & J & 2\Delta_b & 0 \\ 0 & 0 & 0 & 0 & 0 & 0 & J & 0 & 2\Delta_a \end{bmatrix} \tag{4}$$

which is defined based on the bare states mentioned above. Assuming $\Delta_a = \Delta_b = \Delta_1 = \Delta$, the eigenvalues and eigenstates of the system within the two excitation subspace are given by

$$E_0 = 0, |\psi_0\rangle = |0,0,g\rangle \tag{5}$$

$$E_1^0 = \Delta, \left|\psi_1^0\right\rangle = -\frac{J}{\sqrt{g^2+J^2}}|0,0,e\rangle + \frac{g}{\sqrt{g^2+J^2}}|1,0,g\rangle \tag{6}$$

$$E_1^- = -\sqrt{g^2+J^2} + \Delta, |\psi_1^-\rangle = \frac{g}{\sqrt{2J^2+2g^2}}|0,0,e\rangle - \frac{1}{\sqrt{2}}|0,1,g\rangle + \frac{J}{\sqrt{2J^2+2g^2}}|1,0,g\rangle \tag{7}$$

$$E_1^+ = \sqrt{g^2+J^2} + \Delta, |\psi_1^+\rangle = \frac{g}{\sqrt{2J^2+2g^2}}|0,0,e\rangle + \frac{1}{\sqrt{2}}|0,1,g\rangle + \frac{J}{\sqrt{2J^2+2g^2}}|1,0,g\rangle \tag{8}$$

$$E_2^0 = 2\Delta \tag{9}$$

$$E_2^{-} = \frac{1}{2}(-\sqrt{2}\sqrt{2g^2+3J^2-\sqrt{J^2(16g^2+J^2)}}+4\Delta) \tag{10}$$

$$E_2^{--} = \frac{1}{2}(-\sqrt{2}\sqrt{2g^2+3J^2+\sqrt{J^2(16g^2+J^2)}}+4\Delta) \tag{11}$$

$$E_2^{+} = \frac{1}{2}(\sqrt{2}\sqrt{2g^2+3J^2-\sqrt{J^2(16g^2+J^2)}}+4\Delta) \tag{12}$$

$$E_2^{++} = \frac{1}{2}(\sqrt{2}\sqrt{2g^2+3J^2+\sqrt{J^2(16g^2+J^2)}}+4\Delta). \tag{13}$$

The eigenstates corresponding to the eigenvalues E_2^0, E_2^{--}, E_2^{-}, E_2^{+}, and E_2^{++} are too cumbersome. We will not list them here. The transition channels are demonstrated in Figure 2a. The multiple excitation paths from state $|0,0,g\rangle$ to state $|2,0,g\rangle$ are the fundamental and essential factors to the single photon blockade in our system. A single photon blockade is apparent when one can find the proper quantum destructive interference conditions among different transition paths from $|1,0,g\rangle$ to $|2,0,g\rangle$. The eigenenergy levels are shown in Figure 2b. The blue arrows and red arrows illustrate the anharmonicity of the Jaynes–Cummings ladder. When the resonant absorption frequency ω is detuned to reach the state $|\psi_1^-\rangle$ (corresponding to the eigenvalues E_1^-) or $|\psi_1^+\rangle$, it will block the absorption of a second photon at frequency ω because the states corresponding to eigenenergy E_2^{--}, E_2^{-}, E_2^0, E_2^{+}, and E_2^{++} are all detuned from ω.

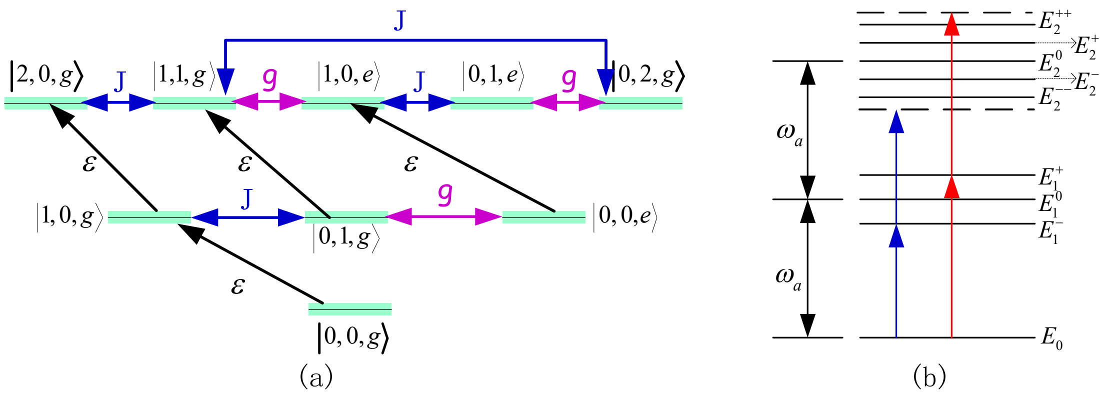

Figure 2. (**a**) Energy levels within two excitation subspaces and the corresponding excitation paths; (**b**) the eigenenergy spectrum of the dressed states within two excitation subspaces.

3. Numerical Computation Conventional and Unconventional Photon Blockade

In this section, we study the conventional and unconventional photon blockade effects by numerically calculating the equal-time second-order correlation function of Cavity A.

3.1. Quantum Master Equation

We assume our system satisfies the Born approximation and is in a "short-memory environment" such that it also satisfies the Markov approximation. The time-evolution of the system density matrix is then governed by the Lindblad master equation [26,27]:

$$\begin{aligned}\dot{\rho} = i[\rho,H] + \tfrac{\kappa_a}{2}(\overline{n}_{tha}+1)\Im[a] + \tfrac{\kappa_a}{2}\overline{n}_{tha}\Im[a^\dagger] + \tfrac{\kappa_b}{2}(\overline{n}_{thb}+1)\Im[b] \\ + \tfrac{\kappa_b}{2}\overline{n}_{thb}\Im[b^\dagger] + \tfrac{\gamma}{2}(\overline{n}_{th1}+1)\Im[\sigma] + \tfrac{\gamma}{2}\overline{n}_{th1}\Im[\sigma^\dagger]\end{aligned} \tag{14}$$

The super operator $\Im[o] = 2o\rho o^\dagger - \rho o^\dagger o - o^\dagger o\rho$ is the Lindblad term [28,29] accounting for the losses to the environment. $\overline{n}_{thx} = [\exp(\hbar\omega_x/K_BT_x)-1]^{-1}$, $x = \{a,b,1\}$ are the average thermal excitation numbers of the bath at temperature T_x, with K_B as the Boltzmann constant. κ_a and κ_b are the dissipation rates of Cavity A and Cavity B, respectively. The transition rate from $|e\rangle$ to $|g\rangle$ of the atom is described by the term proportional to $\frac{\gamma}{2}(\overline{n}_{th1}+1)$, which contains a rate for spontaneous transitions and a rate for stimulated transitions induced by thermal photons. The last term in Equation (14) describes the transition rate from $|g\rangle$ to $|e\rangle$, which is obtained by absorbing thermal photons from the cavity field. At optical frequencies and laboratory temperatures, the thermal photon number $\overline{n}_{thx}$ can be completely negligible [26].

The time evolution of the mean photon numbers in Cavity A can be obtained by solving the master Equation (14). The result is shown in Figure 3 in which Cavity A, Cavity B, and the atom have the same detuning with respect to the driving laser.

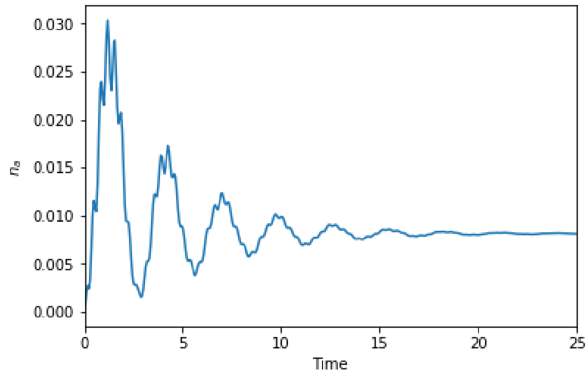

Figure 3. Time evolution of the average photon numbers in Cavity A in unit of $2\pi/\kappa_a$. The parameters are $\kappa_b = \kappa_a$, $\gamma = 0.6\kappa_a$, $\Delta_a = 7\kappa_a$, $\Delta_a = \Delta_b = \Delta_1$, $\varepsilon = 0.5\kappa_a$, $J = 9\kappa_a$, $g = 2\kappa_a$, and $\overline{n}_{tha} = \overline{n}_{thb} = \overline{n}_{th1} = 0$.

The photon-number statistics in Cavity A can be evaluated by the result of the photon correlation function, which is defined in the steady-time limit as

$$g^{(2)}(\tau) = \lim_{t->\infty} \frac{\langle a^\dagger(t)a^\dagger(t+\tau)a(t+\tau)a(t)\rangle}{\langle a^\dagger(t)a(t)\rangle^2}. \tag{15}$$

We assume that there is zero delay between photons, i.e., $\tau = 0$, and Equation (15) can then be simplified to

$$g^{(2)}(0) = \frac{\langle a^\dagger a^\dagger aa\rangle_{ss}}{\langle a^\dagger a\rangle_{ss}^2} \tag{16}$$

where 'ss' means steady state. In the weak excitation limit, $g^{(2)}(0)$ can be roughly estimated by the system density matrix element expanded in the bare state subspace. That is,

$$\left\langle a^\dagger a^\dagger aa\right\rangle_{ss} = Tr(a^\dagger a^\dagger aa\rho_{ss}) \approx \sum_{k=0}^{8}\langle k|a^\dagger a^\dagger aa \sum_{m,n=0}^{8} \rho_{mn}|m\rangle\langle n|k\rangle = 2\rho_{88} \tag{17}$$

$$\begin{aligned} \langle a^\dagger a\rangle_{ss} &= Tr(a^\dagger a\rho_{ss}) \approx \sum_{k=0}^{8}\langle k|a^\dagger a \sum_{m,n=0}^{8}\rho_{mn}|m\rangle\langle n|k\rangle \\ &= \rho_{33}+\rho_{55}+\rho_{66}+2\rho_{88} \approx \rho_{33} \end{aligned} \tag{18}$$

where k in $|k\rangle$ is the index corresponding to the bare states listed in Section 2.

The detuning with respect to the driving light is an important factor affecting the photon blockade effect. We plot the equal-time second-order correlation function $g^{(2)}(0)$ as a function of the scaled detuning Δ/κ_a in Figure 4, where $\Delta = \Delta_a = \Delta_b = \Delta_1$. The red dashed curve in Figure 4 is calculated according to Equations (16)–(18), and the blue curve is obtained by solving Equation (14) numerically. These two curves match well in the parameter domain. Thus, we can analyze the peaks and dips of the second correlation curve based on the profiles of the ρ_{33} and ρ_{88} curves. As shown in Figure 4, $\rho_{33} \gg \rho_{88}$ with $\rho_{33} = \langle 1,0,g|\rho_{ss}|1,0,g\rangle$ and $\rho_{88} = \langle 2,0,g|\rho_{ss}|2,0,g\rangle$. There are three peaks in the ρ_{33} curve that are caused by the resonance transitions of the system. As shown in Figure 2b, there are three resonant transition channels for a single photon, i.e., $|\psi_0\rangle \to |\psi_1^-\rangle$, $|\psi_0\rangle \to |\psi_1^0\rangle$, and $|\psi_0\rangle \to |\psi_1^+\rangle$. The positions of these three peaks can be calculated from the eigenvalues of these states. The positions of the left peak, the middle one, and the right one are obtained based on the resonant transition conditions in the rotating frame $E_1^+ - E_0 = 0$, $E_1^0 - E_0 = 0$, and $E_1^- - E_0 = 0$. According to Equations (5)–(8) and based on parameters used in Figure 4, one can obtain the positions of these three peaks: -9.1782, 0, and 9.1782. The five peaks in the ρ_{88} curve are caused by the resonant transition of two photons, whose position can be calculated in the same way as those in the ρ_{33} curve, and the values are -6.6446, -4.2683, 0, 4.2683, and 6.6446, respectively. The other two peaks in the ρ_{88} curve, whose positions are the same as the left one and right one in the ρ_{33} curve, are induced by a single photon resonant transition. The dips in the ρ_{33} and ρ_{88} curves are induced by the destructive quantum interference effect between different transition paths, as shown in Figure 2b. The locations of the two peaks in the correlation function $g^{(2)}(0)$ correspond to the two dips in the ρ_{33} curve, where the excitation of the single photon resonant transition is low. There is a single photon resonant transition and a two-photon resonant transition at $\Delta/\kappa_a = 0$ in the ρ_{33} and ρ_{88} curves. The dip at $\Delta/\kappa_a = 0$ in the correlation function $g^{(2)}(0)$ curve means the single photon resonant transition is far stronger than the two-photon resonant transition at that position. The locations of the other dips in the $g^{(2)}(0)$ curve correspond to those in the ρ_{88} curve.

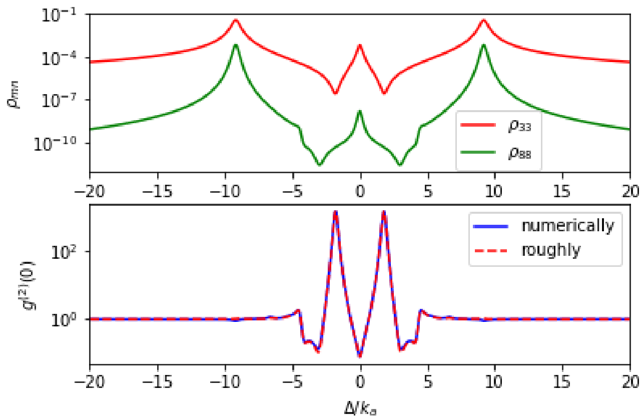

Figure 4. Plots of the density matrix element ρ_{33}, ρ_{88} and the second-order correlation function $g^{(2)}(0)$ as functions of the scaled detuning of Cavity A for $\varepsilon = 0.1\kappa_a$ and $g = 1.8\kappa_a$. Other parameters are the same as in Figure 3.

To investigate the influence of the coupling strength g and the hopping interaction strength J on the correlation function, in Figure 5, we plot the equal-time second correlation function as the two scaled parameters, g/κ_a and J/κ_a, with the fixed detuning $\Delta = 0$, which is a detuning of the single photon resonant transition. From Figure 5, we can see that, when the coupling strength between Cavity B and the atom is larger than κ_a, i.e., $g/\kappa_a > 1$, one can obtain a minimum value of $g^{(2)}(0)$ at the ratio between the hopping interaction strength and the coupling strength $J/g \approx 1.25$. At this ratio, the two photon transition is suppressed and the single photon transition is far stronger. As illustrated in Figure 5, two-photon antibunching can also be obtained when the coupling strength between Cavity B and the atom is weaker than the decay rate of Cavity A. That is, the single photon blockade effect can be obtained in our system under weak nonlinearity, which is induced by the atom in Cavity B in our system with $g < \kappa_a$. Around the other region at $g \approx 0.5\kappa_a$, one can obtain a low value of $g^{(2)}(0)$ as described in Figure 5. However, if we continue to decrease the coupling strength below $0.3\kappa_a$, the photon blockade effect will disappear, and a two-photon bunching effect will become obvious.

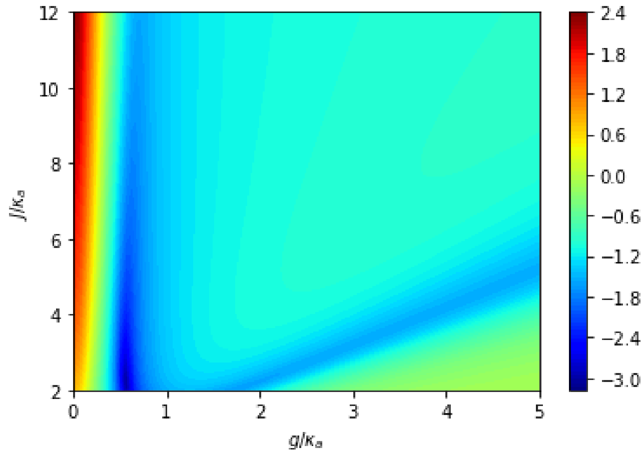

Figure 5. The equal-time second-order correlation function $g^{(2)}(0)$ as a function of the scaled coupling strength g/κ_a and the scaled hopping interaction strength J/κ_a under the resonant condition $\Delta = \Delta_a = \Delta_b = \Delta_1 = 0$. Other parameters are the same as in Figure 4.

3.2. Unconventional Photon Blockade with Atom-Cavity Detuning

In this section, we focus on the unconventional photon blockade when Cavity A, Cavity B, and the atom are out-of resonance based on weak nonlinearities. By solving Equation (14) numerically, we plot the equal-time second order correlation function $\log_{10} g^{(2)}(0)$ as a function of the scaled cavity detuning Δ/κ_a and the scaled atom detuning Δ_1/κ_a in Figure 6, where Cavity B is resonant with Cavity A. Based on the parameters of Figure 6, when the atom is weakly coupled to Cavity B by $g = 0.67\kappa_a$ and the interaction strength between the two cavities is $J = 2\kappa_a$, one can obtain an irregular single photon blockade region at the center of the figure while the detuning of Cavity A, Cavity B, and the atom are all within $[-2\kappa_a, +2\kappa_a]$. By increasing the coupling strength and the hopping strength to $g = 0.8\kappa_a$ and $J = 4\kappa_a$, we can obtain the other two symmetric photon block detuning regimes located at about $[-\kappa_a, -3\kappa_a]$ and $[+\kappa_a, +3\kappa_a]$, as shown in Figure 6b. With the fixed coupling strength $g = 0.67\kappa_a$ and based on the condition that the atom in Cavity B is resonant with the driving laser, i.e., $\Delta_1 = 0$, Figure 7 shows the correlation function $\log_{10} g^{(2)}(0)$ as a function of different detunings of Cavities A and B for photon hopping strength between the two cavities $J = 3\kappa_a$ in Figure 7a and $J = 6\kappa_a$ in Figure 7b. One can see from Figure 7 that the single photon blocked region ($\log_{10} g^{(2)}(0) < 0$) is symmetrical and centered on $\Delta_a = 0$ and $\Delta_b = 0$. As the moderate increase of the hopping strength J, the single photon blocked region stretches to both the red sideband and blue sideband of Cavity A.

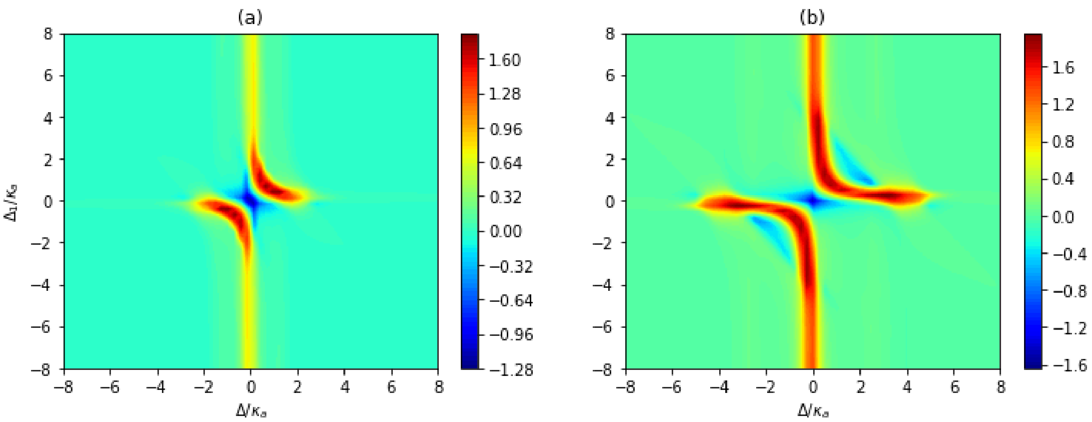

Figure 6. The equal-time second-order correlation function $\log_{10} g^{(2)}(0)$ as a function of the scaled detuning $\Delta/\kappa_a = \Delta_a/\kappa_a = \Delta_b/\kappa_a$ and Δ_1/κ_a for (**a**) $g = 0.67\kappa_a$ and $J = 2\kappa_a$; (**b**) $g = 0.8\kappa_a$ and $J = 4\kappa_a$. Other parameters are the same as in Figure 4.

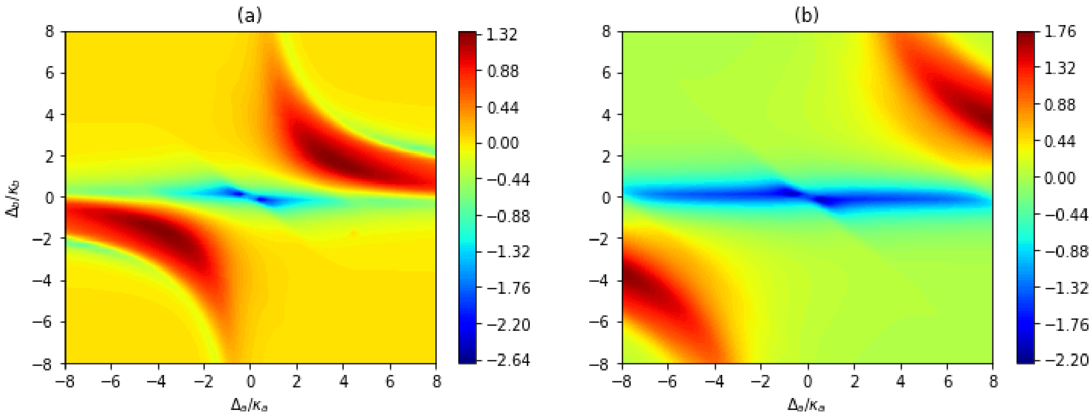

Figure 7. The equal-time second-order correlation function $\log_{10} g^{(2)}(0)$ as a function of scaled detuning Δ_a/κ_a and Δ_b/κ_b under the condition of the atom resonant with the driving laser $\Delta_1 = 0$ for (**a**) $J = 3\kappa_a$ and (**b**) $J = 6\kappa_a$. Other parameters are the same as in Figure 6a.

4. Optimal Parameters for Sub-Poissonian Characters Derived by the Non-Hermitian Effective Hamiltonian Method

In this section, we focus on the analytical optimal conditions for the system parameters that maximize the sub-Poissonian character of Cavity A. In the weak driving limit, the system states can be expressed as an expansion on the bare states mentioned in Section 2:

$$\begin{aligned} |\psi(t)\rangle &= c_{000}|00g\rangle + c_{001}|00e\rangle + c_{010}|01g\rangle + c_{100}|10g\rangle \\ &+ c_{011}|01e\rangle + c_{101}|10e\rangle + c_{110}|11g\rangle + c_{020}|02g\rangle + c_{200}|20g\rangle \end{aligned} \tag{19}$$

The system is governed by a stochastic Schrodinger equation as (assuming $\hbar = 1$)

$$i\frac{d}{dt}|\psi(t)\rangle = H_{eff}|\psi(t)\rangle \tag{20}$$

where the non-Hermitian effective Hamiltonian [17,18,26] can be written as

$$\begin{aligned} H_{eff} &= (\Delta_a - i\tfrac{\kappa_a}{2})a^\dagger a + (\Delta_b - i\tfrac{\kappa_b}{2})b^\dagger b + (\Delta_1 - i\tfrac{\gamma}{2})\sigma^\dagger\sigma \\ &+ g(\sigma^\dagger b + \sigma b^\dagger) + J(a^\dagger b + ab^\dagger) + \varepsilon(a^\dagger + a) \end{aligned} \tag{21}$$

Here, we consider the system evolution under the condition that the three components Cavity A, Cavity B, and the atom are resonant, i.e., $\Delta_a = \Delta_b = \Delta_1 = \Delta$, and the bandwidth of Cavity A equals that of Cavity B, i.e., $\kappa_a = \kappa_b = \kappa$. The time-dependent coefficients $c_{mnp}(t)$ can be obtained from Equations (20) and (21). According to the idea of performing a consistent expansion of the elements to dominant order in powers of ε/κ_a [30], we neglect the subleading order in the driving laser amplitude and obtain the equations of $c_{mnp}(t)$:

$$i\dot{c}_{001} = (\Delta - i\frac{\gamma}{2})c_{001} + gc_{010} \tag{22}$$

$$i\dot{c}_{010} = (\Delta - i\frac{\kappa}{2})c_{010} + gc_{001} + Jc_{100} \tag{23}$$

$$i\dot{c}_{100} = (\Delta - i\frac{\kappa}{2})c_{100} + Jc_{010} + \varepsilon c_{000} \tag{24}$$

$$i\dot{c}_{011} = (\Delta - i\frac{\kappa}{2})c_{011} + (\Delta - i\frac{\gamma}{2})c_{011} + \sqrt{2}gc_{020} + Jc_{101} \tag{25}$$

$$i\dot{c}_{101} = (\Delta - i\frac{\kappa}{2})c_{101} + (\Delta - i\frac{\gamma}{2})c_{101} + gc_{110} + Jc_{011} + \varepsilon c_{001} \tag{26}$$

$$i\dot{c}_{110} = (2\Delta - i\kappa)c_{110} + gc_{101} + \sqrt{2}Jc_{020} + \sqrt{2}Jc_{200} + \varepsilon c_{010} \tag{27}$$

$$i\dot{c}_{020} = (2\Delta - i\kappa)c_{020} + \sqrt{2}gc_{011} + \sqrt{2}Jc_{110} \tag{28}$$

$$i\dot{c}_{200} = (2\Delta - i\kappa)c_{200} + \sqrt{2}Jc_{110} + \sqrt{2}\varepsilon c_{100}. \tag{29}$$

The relationship between different $c_{mnp}(t)$ in Equations (22)–(29) once again illustrates the multi-transition channels between different system states, which is consistent with that in Figure 2a. The amplitudes of the coefficient $c_{mnp}(t)$ in Equation (19) can be divided into three levels with respect to ε/κ_a. That is, the amplitudes of $c_{000}(t)$ is of the zero order of ε/κ_a, $\{c_{001}(t), c_{010}(t)$, and $c_{100}(t)\}$ of the first order and $\{c_{011}(t), c_{101}(t), c_{110}(t), c_{020}(t), c_{200}(t)\}$ of the second order, i.e., $c_{000}(t) \gg c_{001}(t), c_{010}(t), c_{100}(t) \gg c_{011}(t), c_{101}(t), c_{110}(t), c_{020}(t), c_{200}(t)$. The average photon occupations in Cavity A and the equal-time second-order correlations then approximate to

$$n_a = \left\langle a^\dagger a \right\rangle = \left|c_{100}\right|^2 + \left|c_{101}\right|^2 + \left|c_{110}\right|^2 + 2\left|c_{200}\right|^2 \simeq \left|c_{100}\right|^2 \tag{30}$$

$$g^{(2)}(0) = \frac{\langle a^\dagger a^\dagger a a \rangle}{n_a^2} \simeq 2\frac{|c_{200}|^2}{|c_{100}|^4}. \tag{31}$$

The expressions of c_{100} and c_{200} can be obtained by solving Equations (22)–(29) for the steady state $|\psi\rangle_{ss}$ with $\dot{c}_{mnp} = 0$ and $c_{000} = 1$.

$$c_{100} = \frac{2[-4ig^2 + (\gamma + 2i\Delta)(-i\kappa + 2\Delta)]\varepsilon}{4g^2(\kappa + 2i\Delta) + [4J^2 + (\kappa + 2i\Delta)^2(\gamma + 2i\Delta)]} \tag{32}$$

$$c_{200} = -2\sqrt{2}\left\{32g^6 + 2g^2X_1^2(16J^2 + X_2) - 8g^4(4J^2 - X_1X_3) + X_1^3X_5\right\}\varepsilon^2 M^{-1} \tag{33}$$

$$\begin{aligned} M \; &= 32g^6X_1^2 + 2g^2(4J^2 + X_1^2)(X_1^2X_2 + 4J^2X_4) \\ &+8g^4X_1[X_1^2X_3 + J^2(8\gamma - 4\kappa + 8i\Delta)] + X_5[4J^2 + X_1^2]^2X_1 \end{aligned} \tag{34}$$

where, $X_1 = \kappa + 2i\gamma\Delta$, $X_2 = 2\kappa^2 + 7\kappa\gamma + 5\gamma^2 + 22i\kappa\Delta + 34i\gamma\Delta - 56\Delta^2$, $X_3 = 3\kappa + 4\gamma + 14i\Delta$, $X_4 = 2\kappa^2 - \kappa\gamma + \gamma^2 + 6i\kappa\Delta + 2i\gamma\Delta - 8\Delta^2$ and $X_5 = [4J^2 + (\kappa + \gamma + 4i\Delta)^2](\gamma + 2i\Delta)$.

The optimal parameter for single photon blockade in Cavity A can be obtained by set $c_{200} = 0$ under the condition $c_{100} \neq 0$. Based on Equation (33), one can obtain the optimal parameter pairs of the coupling strength g and the detuning Δ with fixed hopping strength J and atom decay rate γ. When J is fixed at $2.5\kappa_a$ and $\gamma = 0.6\kappa_a$, we can obtain the real solution of the optimal parameter pairs $\{\{g \to -7.63415\kappa_a, \Delta \to -6.89979\kappa_a\}, \{g \to -7.63415\kappa_a, \Delta \to 6.89979\kappa_a\}, \{g \to -0.924508\kappa_a, \Delta \to -1.32075\kappa_a\}, \{g \to -0.924508\kappa_a, \Delta \to 1.32075\kappa_a\}, \{g \to 0.924508\kappa_a, \Delta \to -1.32075\kappa_a\}, \{g \to 0.924508\kappa_a, \Delta \to 1.32075\kappa_a\}, \{g \to 7.63415\kappa_a, \Delta \to -6.89979\kappa_a\}, \{g \to 7.63415\kappa_a, \Delta \to 6.89979\kappa_a\}\}$.

We verify the solution by plotting the equal-time second-order correlation function $g^{(2)}(0)$ as a function of the scaled detuning for different coupling strength g in Figure 8. As expected, the values of $g^{(2)}(0)$ are much smaller when we use the $\{g, \Delta\}$ pairs listed above than others, i.e., it shows two strong photon antibunching effects at $\Delta \simeq 1.3\kappa_a$ with $g = 0.924508\kappa_a$ in Figure 8a and $\Delta \simeq 6.9\kappa_a$ with $g = 7.63415\kappa_a$ in Figure 8b. We also see the symmetric property from optimal $\{g, \Delta\}$ solutions, that is, when the coupling strength g is fixed at one of the optimal values, there are two symmetric optimal detunings for Cavity A, Cavity B, and the atom with respect to the driving laser, and vice versa. The underlying physical mechanism of the optimal solution for a single photon blockade lies in the destructive interference between different paths of two photon excitation in Cavity A. As illustrated in Figure 2a and Equation (29), the occupation of $|2, 0, g\rangle$ can be minimized by reducing the contribution from $|1, 0, g\rangle$ and $|1, 1, g\rangle$. When destructive interference between the direct excitation path $|0, 0, g\rangle \to |1, 0, g\rangle \to |2, 0, g\rangle$ and the indirect excitation paths $|0,0,g\rangle \to |1,0,g\rangle \to |0,1,g\rangle \to |0,0,e\rangle \to (|1,0,e\rangle \leftrightarrow |0,1,e\rangle \leftrightarrow |0,2,g\rangle \leftrightarrow |1,1,g\rangle) \to |2,0,g\rangle$ occurs, the occupation of $|2,0,0\rangle$ will be reduced; hence, the value of $g^{(2)}(0)$ is decreased.

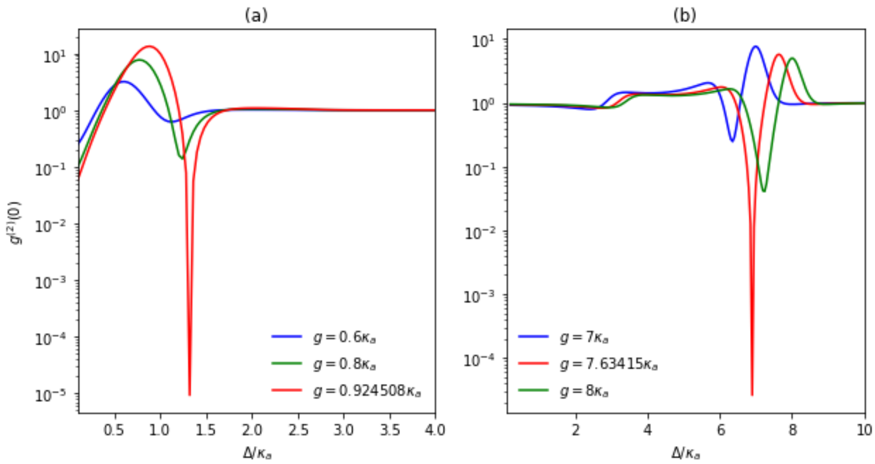

Figure 8. Plots of equal-time second-order correlation function $g^{(2)}(0)$ as a function of the scaled detuning for (**a**) $g = 0.6\kappa_a$, $g = 0.8\kappa_a$, and $g = 0.924508\kappa_a$; (**b**) $g = 7\kappa_a$, $g = 7.63415\kappa_a$, and $g = 8\kappa_a$ with fixed $J = 2.5\kappa_a$. Other parameters are the same as in Figure 4.

Figure 9 shows several optimal $\{g, \Delta\}$ pairs for different atom decay rate γ. When $\gamma = 0.25\kappa_a$, one can get $\{\{g \to \pm 0.782092\kappa_a, \Delta \to \pm 1.19804\kappa_a\}, \{g \to \pm 7.89333\kappa_a, \Delta \to \pm 7.17599\kappa_a\}\}$, and $\{\{g \to \pm 0.817538\kappa_a, \Delta \to \pm 1.22938\kappa_a\}, \{g \to \pm 7.81893\kappa_a, \Delta \to \pm 7.09409\kappa_a\}\}$ with $\gamma = 0.35\kappa_a$, $\{\{g \to \pm 0.857111\kappa_a, \Delta \to \pm 1.26361\kappa_a\}, \{g \to \pm 7.74537\kappa_a, \Delta \to \pm 7.01522\kappa_a\}\}$ with $\gamma = 0.45\kappa_a$. As shown in Figure 9, with the increase in the atom lifetime, the optimal coupling strength g decreases in the UPB regime where $g < \kappa_a$ and increases in the conventional photon blockade regime where $g > \kappa_a$.

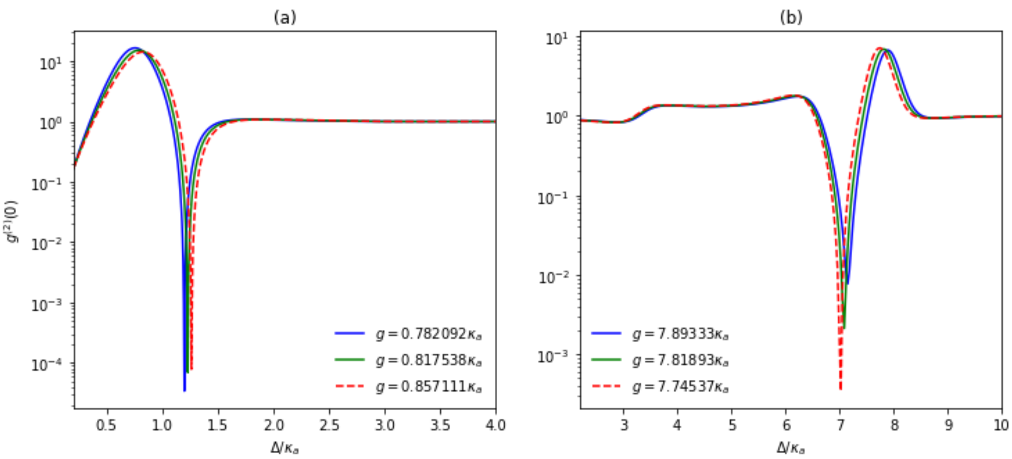

Figure 9. Plots of $g^{(2)}(0)$ versus the scaled detuning Δ/κ_a for (**a**) $g < \kappa_a$; (**b**) $g > \kappa_a$ with $\gamma = 0.25\kappa_a$, $\gamma = 0.35\kappa_a$, and $\gamma = 0.45\kappa_a$. Other parameters are the same as in Figure 8.

5. Supplementary Discussion

In the above sections, we find that Cavity A is weakly driven by a continuous laser field and Cavity B is not. If the cavities in our system are both driven by a laser field, the Hamiltonian of the system reads

$$H = \Delta_a a^\dagger a + \Delta_b b^\dagger b + \Delta_1 \sigma^\dagger \sigma + g(\sigma^\dagger b + \sigma b^\dagger) + J(a^\dagger b + a b^\dagger) + \varepsilon_a(a^\dagger + a) + \varepsilon_b(b^\dagger + b). \tag{35}$$

There will then also be direct and indirect excitation paths from state $|0,0,g\rangle$ to $|0,2,g\rangle$, which provides a fundamental condition for the photon blockade in Cavity B.

We plot the equal-time second-order correlation function in Figure 10 as a function of the two scaled parameters g/κ_a and J/κ_a under the condition that the two driving lasers are of the same frequency. With zero detuning, i.e., Cavity A, Cavity B, and the atom are resonant with the pump laser; we can see from Figure 10 that there is a single photon blockade in both Cavity A and Cavity B. However, the parameter regimes for the photon blockade are different in Cavity A and Cavity B. As shown in Figure 10a, the two-photon antibunching effect is apparent in Cavity A when $g \geq \kappa_a$ and the ratio between J and g is approximately equal to one for a minimum $g^{(2)}(0)$, whereas the photon blockade effect in Cavity B appears when $g < \kappa_a$ (κ_b) with $J > g$. We obtain two different types of photon blockades at the same time: a conventional photon blockade is apparent in the linear cavity A and an unconventional photon blockade is dominant in the nonlinear cavity B, here Cavity A, Cavity B, and the atom in Cavity B are all resonant with the pump laser.

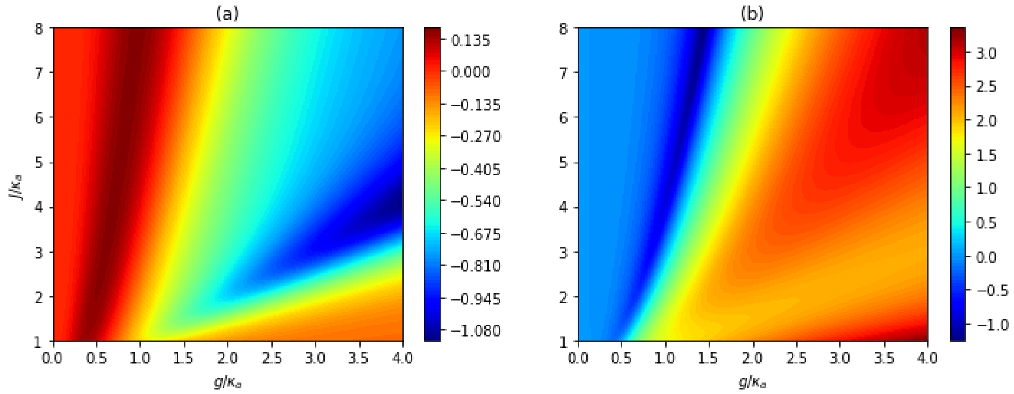

Figure 10. Plots of equal-time second-order correlation function $g^{(2)}(0)$ of (**a**) Cavity A and (**b**) Cavity B as a function of scaled atom-cavity coupling strength g/κ_a and cavity interaction strength J/κ_a for $\kappa_b = \kappa_a$, $\gamma = 0.6\kappa_a$, $\varepsilon_a = \varepsilon_b = 0.1\kappa_a$, and $\Delta_a = \Delta_b = \Delta_1 = 0$.

6. Conclusions

In summary, we have studied the photon statistics of a coupled cavity QED system that consists of a linear cavity and a nonlinear cavity that consists of a two-level atom. The linear cavity is weakly driven by a continuous laser field, and the two cavities are coupled by hopping strength J. The single photon blockade effect can be observed in the linear cavity, both conventional and unconventional. Compared with existing schemes, we can achieve a conversion between a conventional photon blockade and an unconventional photon blockade in the same system; more importantly, we can also achieve the coexistence of two different photon blockades. In addition, we obtain the coupling between two cavities via photon hopping interactions, which can be realized by current experimental techniques. The photon blockade provides an effective method for obtaining a single photon source, which is the basis of realizing optical quantum information technology. Thus, our work has potential applications in quantum information processing and quantum communication. Being a theoretical work, we provide detailed theoretical derivation and numerical analysis. In our model, these photon blockade effects are mainly achieved by the quantum destructive interference between different excitation paths. We have analyzed the values of the equal-time second-order correlation function in the truncated Hilbert space by solving the master equation of the coupled cavities. In the same parameter regime, we also derived the optimal atom-cavity coupling strength and cavity detuning parameter pairs, which once again verify the symmetric photon blockade regime for the linear cavity. We also extend our model by adding a pump laser to Cavity B. We find that, under the condition of driving these two cavities simultaneously, the conventional photon blockade in Cavity A is dominant, while in Cavity B the unconventional photon blockade is apparent. In our scheme, the introduction of a two-level atom provides an efficient method for the realization of an unconventional photon blockade in Cavity B. When Cavity B is manipulated by the pump laser, the interaction between the cavity and atom can be effectively controlled, which may affect the nonlinearity of the total system. Thus, we obtain the unconventional photon blockade in the case of weak nonlinearity. Here the pump laser and the two-level atom are well controlled experimentally, and the unconventional photon blockade is not obviously dependent on the decay rate of cavity. Therefore, we provide a feasible scheme for the realization of an unconventional photon blockade.

Author Contributions: Conceptualization, M.-C.L. and A.-X.C.; methodology, A.-X.C.; software, M.-C.L.; formal analysis, M.-C.L.; writing—original draft preparation, M.-C.L.; writing—review and editing, A.-X.C.; supervision, A.-X.C.

Funding: This work was supported by the project of National Natural Science Foundation of China [grant number 11775190] and by Science and Technology of Jiangxi province [grant number 20171BAB212006]; the project of science and technology awarded by the Education Bureau of Jiangxi Province [grant number JJ160503] and by the Science Foundation of Zhejiang SCI-TECH University (17062071-Y).

Conflicts of Interest: The authors declare no conflict of interest.

References

1. Hadfield, R.H. Single-photon detectors for optical quantum information applications. *Nat. Photonics* **2009**, *3*, 696–705. [CrossRef]
2. Eisaman, M.D.; Fan, J.; Migdall, A.; Polyakov, S.V. Invited review article: Single-photon sources and detectors. *Rev. Sci. Instrum.* **2011**, *82*, 071101. [CrossRef] [PubMed]
3. Lounis, B.; Orrit, M. Single-photon sources. *Rep. Prog. Phys.* **2005**, *68*, 1129–1179. [CrossRef]
4. Clauser, J.F. Experimental distinction between the quantum and classical field-theoretic predictions for the photoelectric effect. *Phys. Rev. D* **1974**, *9*, 853. [CrossRef]
5. Diedrich, F.; Walther, H. Nonclassical radiation of a single stored ion. *Phys. Rev. Lett.* **1987**, *58*, 203–206. [CrossRef] [PubMed]
6. De Martini, F.; Di Giuseppe, G.; Marrocco, M. Single-mode generation of quantum photon states by excited single molecules in a microcavity trap. *Phys. Rev. Lett.* **1996**, *76*, 900–903. [CrossRef] [PubMed]
7. Lounis, B.; Moerner, W.E. Single photons on demand from a single molecule at room temperature. *Nature* **2000**, *407*, 491–493. [CrossRef]
8. Brouri, R.; Beveratos, A.; Poizat, J.P.; Grangier, P. Photon antibunching in the fluorescence of individual color centers in diamond. *Opt. Lett.* **2000**, *25*, 1294–1296. [CrossRef]
9. Michler, P.; Imamoğlu, A.; Mason, M.D.; Carson, P.J.; Strouse, G.F.; Buratto, S.K. Quantum correlation among photons from a single quantum dot at room temperature. *Nature* **2000**, *406*, 968–970. [CrossRef]
10. He, Y.M.; He, Y.; Wei, Y.J.; Wu, D.; Atatüre, M.; Schneider, C.; Höfling, S.; Kamp, M.; Lu, C.Y.; Pan, J.W. On-demand semiconductor single-photon source with near-unity indistinguishability. *Nat. Nanotechnol.* **2013**, *8*, 213–217. [CrossRef]
11. Gschrey, M.; Thoma, A.; Schnauber, P.; Seifried, M.; Schmidt, R.; Wohlfeil, B.; Krüger, L.; Schulze, J.H.; Heindel, T.; Burger, S.; et al. Highly indistinguishable photons from deterministic quantum-dot microlenses utilizing three-dimensional in situ electron-beam lithography. *Nat. Commun.* **2015**, *6*, 7662. [CrossRef] [PubMed]
12. Imamoğlu, A.; Schmidt, H.; Woods, G.; Deutsch, M. Strongly interacting photons in a nonlinear cavity. *Phys. Rev. Lett.* **1997**, *79*, 1467. [CrossRef]
13. Leoński, W.; Tanaś, R. Possibility of producing the one-photon state in a kicked cavity with a nonlinear Kerr medium. *Phys. Rev. A* **1994**, *49*, R20–R23. [CrossRef] [PubMed]
14. Birnbaum, K.M.; Boca, A.; Miller, R.; Boozer, A.D.; Northup, T.E.; Kimble, H.J. Photon blockade in an optical cavity with one trapped atom. *Nature* **2005**, *436*, 87–90. [CrossRef] [PubMed]
15. Peyronel, T.; Firstenberg, O.; Liang, Q.Y.; Hofferberth, S.; Gorshkov, A.V.; Pohl, T.; Lukin, M.D.; Vuletić, V. Quantum nonlinear optics with single photons enabled by strongly interacting atoms. *Nature* **2012**, *488*, 57–60. [CrossRef] [PubMed]
16. Liew, T.C.H.; Savona, V. Single photons from coupled quantum modes. *Phys. Rev. Lett.* **2010**, *104*, 183601. [CrossRef] [PubMed]

17. Flayac, H.; Savona, V. Unconventional photon blockade. *Phys. Rev. A* **2017**, *96*, 053810. [CrossRef]
18. Bin, Q.; Lü, X.Y.; Bin, S.W.; Wu, Y. Two-photon blockade in a cascaded cavity-quantum-electrodynamics system. *Phys. Rev. A* **2018**, *98*, 043858. [CrossRef]
19. Bamba, M.; Imamoğlu, A.; Carusotto, I.; Ciuti, C. Origin of strong photon antibunching in weakly nonlinear photonic molecules. *Phys. Rev. A* **2011**, *83*, 021802. [CrossRef]
20. Zou, F.; Lai, D.G.; Liao, J.Q. Photon blockade effect in a coupled cavity system. *arXiv*, 2018; arXiv:1803.06642.
21. Xu, X.W.; Li, Y. Tunable photon statistics in weakly nonlinear photonic molecules. *Phys. Rev. A* **2014**, *90*, 043822. [CrossRef]
22. Shen, H.Z.; Zhou, Y.H.; Yi, X.X. Tunable photon blockade in coupled semiconductor cavities. *Phys. Rev. A* **2015**, *91*, 063808. [CrossRef]
23. Flayac, H.; Gerace, D.; Savona, V. An all-silicon single-photon source by unconventional photon blockade. *Sci. Rep.* **2015**, *5*, 11223. [CrossRef] [PubMed]
24. Gerace, D.; Savona, V. Unconventional photon blockade in doubly resonant microcavities with second-order nonlinearity. *Phys. Rev. A* **2014**, *89*, 031803. [CrossRef]
25. Tang, J.; Geng, W.; Xu, X. Quantum interference induced photon blockade in a coupled single quantum dot-cavity system. *Sci. Rep.* **2015**, *5*, 9252. [CrossRef] [PubMed]
26. Carmichael, H. Master equations and source. In *An Open Systems Approach to Quantum Optics*; Springer: Berlin/Heidelberg, Germany, 1993; pp. 22–35.
27. Breuer, H.P.; Petruccione, F. Quantum master equations. In *The Theory of Open Quantum Systems*; Oxford University Press: Oxford, UK, 2002; pp. 109–216.
28. Carmichael, H.J. Quantum trajectory theory for cascaded open systems. *Phys. Rev. Lett.* **1993**, *70*, 2273–2276. [CrossRef] [PubMed]
29. Johansson, J.R.; Nation, P.D.; Nori, F. QuTiP: An open-source Python framework for the dynamics of open quantum systems. *Comput. Phys. Commun.* **2012**, *183*, 1760–1772. [CrossRef]
30. Carmichael, H.J.; Brecha, R.J.; Rice, P.R. Quantum interference and collapse of the wavefunction in cavity QED. *Opt. Commun.* **1991**, *82*, 73–79. [CrossRef]